Electronic Supplementary Information

Formation of paired Ga sites in CHA-type zeolite frameworks via transcription-induced method

Takumi Kaneko,[a] Mizuho Yabushita,[a,*] Ryota Osuga,[b] Yugo Sawada,[a] Kei Sato,[a] Ben Liu,[a]

Yoshinao Nakagawa,[a] Kiyotaka Nakajima,[b] Keiichi Tomishige[a,c,*]

[a]*Department of Applied Chemistry, School of Engineering, Tohoku University, 6-6-07 Aoba, Aramaki, Aoba-ku, Sendai, Miyagi 980-8579, Japan*

[b]*Institute for Catalysis, Hokkaido University, Kita 21 Nishi 10, Kita-ku, Sapporo, Hokkaido 001-0021, Japan*

[c]*Advanced Institute for Materials Research (WPI-AIMR), Tohoku University, 2-1-1 Katahira, Aoba-ku, Sendai, Miyagi 980-8577, Japan*

**Corresponding authors: m.yabushita@tohoku.ac.jp (M.Y.); tomishige@tohoku.ac.jp (K.T.)*

[Experimental]

1. Reagents

All the reagents described here were used as-received without further purification. Tetraethyl orthosilicate (TEOS; FUJIFILM Wako Pure Chemical), propylene glycol (PG; FUJIFILM Wako Pure Chemical), an aqueous HNO_3 solution (1 M, FUJIFILM Wako Pure Chemical), $Ga(NO_3)_3$•xH_2O (x = 7–9, FUJIFILM Wako Pure Chemical), citric acid (CA; anhydrous, Nacalai Tesque), ethylene glycol (EG; FUJIFILM Wako Pure Chemical), silica gel (CARiACT G-6, Fuji Silysia Chemical), an aqueous NaOH solution (8 M, FUJIFILM Wako Pure Chemical), an aqueous *N*,*N*,*N*-trimethyl-1-adamantylammonium hydroxide solution (TMAdaOH; 25 wt%, Tokyo Chemical Industry) were employed for synthesizing the Ga-rich amorphous silica-gallia and **CHA**-type zeolites. An aqueous KOH solution (1 M, FUJIFILM Wako Pure Chemical), an aqueous HNO_3 solution (0.5 M, FUJIFILM Wako Pure Chemical), and an aqueous HF solution (47–49 wt%) were used to dissolve each sample prior to the quantitative analysis for Si, Ga, and Co.

2. Synthesis of Ga-rich amorphous silica-gallia via Pechini method

The whole procedure including this and next sections is summarized in Fig. S1. The Ga-rich amorphous silica-gallia sample that was employed as a precursor to Ga-substituted **CHA**-type zeolites in the hydrothermal process was prepared via the Pechini method (also called polymerized complex method)[S1,S2]. Initially, TEOS was transformed into propylene glycol-modified silane (PGMS)[S3] to hamper the undesired evaporation and hydrolysis of TEOS, leading to the ease of handling for the source of Si atoms in the following procedure. Thus, a mixture consisting of TEOS (0.1 mol) and PG (0.4 mol) was stirred in an eggplant flask immersed in an oil bath at 353 K for 24 h. Then, 1 mL of an aqueous HNO_3 solution (1 M) was added into the mixture, which was further stirred at 353 K for 1 h to cause the ligand exchange. The resulting colorless and transparent solution was transferred into a 200 mL volumetric flask and diluted with distilled water to obtain a 0.5 M aqueous PGMS solution.

The thus-prepared aqueous PGMS solution, EG, and CA were mixed in a 500 mL beaker at 333 K to obtain a transparent solution. Note that in the following procedure, the beaker was kept unwrapped in order to evaporate water completely during the heating process. After the addition of $Ga(NO_3)_3$•nH_2O, the entire mixture was stirred again at 333 K to dissolve all solids. In this liquid mixture, the molar ratio of PGMS, $Ga(NO_3)_3$•xH_2O, CA, and EG was 2/1/160/480. The mixture was then heated in a heating mantle at 373 K for *ca.* 1 h to remove water and subsequently at 423 K to induce condensation between EG and CA, obtaining a resin containing Si and Ga atoms. Afterward, the temperature was increased step-by-step from 423 to 723 K to carbonize the resin. The resulting black powder, a composite of silica-gallia and carbonized resin, was ground on a mortar and calcined in an electric furnace in air at 1073 K for 12 h to combust the carbonized resin and yield the white silica-gallia powder. The actual Si/Ga ratio of this silica-gallia specimen was determined by inductively coupled plasma-optical emission spectroscopy (ICP-OES) to be 1.9 after its complete dissolution in an aqueous KOH solution (the detailed procedure for ICP-OES is described below).

3. Hydrothermal synthesis of CHA-type zeolites from Ga-rich amorphous silica-gallia

CHA-type zeolites were synthesized using the Ga-rich amorphous silica-gallia (*vide supra*) under seed-assisted hydrothermal conditions by modifying previously reported procedure.[S4,S5] Initially, silica gel (an

additional Si source to adjust the Si/Ga ratio in the synthesis gels), an aqueous NaOH solution, an aqueous TMAdaOH solution (an organic SDA), and distilled water were charged into a Teflon-lined high-pressure reactor (RW-20, HIRO Company, inner volume 20 mL). The mixture was stirred at room temperature for t_1 hours. After the addition of the Ga-rich amorphous silica-gallia into the gel as a source of both Si and Ga, the resulting synthesis gel was further aged at room temperature for t_2 hours. Note that in all cases in this study, the total aging time (*i.e.*, $t_1 + t_2$) was 48 h, and the molar ratio of Si/Ga/NaOH/TMAdaOH/H_2O of the gel was 1/0.10/0.44/0.20/30. Just before the hydrothermal treatment, a **CHA**-type zeolite seed crystal (whose loading corresponded to 5 wt% against the total weight of SiO_2) was added into the mixture. The hydrothermal process for the gels was conducted using an electric furnace (HIRO Company), which was pre-heated at 443 K to minimize the temperature ramp time, at a tumbling speed of 40 rpm at 443 K for specific times (typically 3 days). After cooling to room temperature, the solid product was separated and washed with distilled water by suction filtration, dried at 333 K overnight, and calcined in air at 873 K for 12 h to remove TMAdaOH and obtain Ga-containing **CHA**-type zeolites. The samples thus prepared were denoted by using t_2 as [Ga]-CHA-t_2. The solid yield was calculated from the division of the weight of calcined [Ga]-CHA-t_2 sample by the total weight of silica gel, Ga-rich silica-gallia, and seed crystal.

4. Characterization of synthesized samples

The contents of Si, Ga, and Co were determined by ICP-OES (iCAP6500, Thermo Fisher Scientific). Prior to analysis, each sample was dissolved completely in 10 mL of an aqueous KOH solution (1 M) at room temperature, and then 5 mL of the solution was diluted 10 times with distilled water. The resultant diluted solution was used for analysis. The crystal structure of the samples was analyzed by powder X-ray diffraction measurement (XRD; MiniFlex600, Rigaku, Cu Kα radiation at 40 kV and 40 mA, scan speed 10° min^{-1}). Relative crystallinity was calculated by using the following equation that was also used in previous report.[S6] In this equation, total peak area was calculated as the sum of area of three peaks at 20.9°, 25.0°, and 26.3°, and [Ga]-CHA synthesized in the hydrothermal treatment time of 3 days was used as the reference sample since this specimen provided the highest peak height in XRD (see Fig. S3A).

$$\text{Relative crystallinity (\%)} = \frac{\text{Total area of peaks at 20.9°, 25.0°, and 26.3° of the synthesized sample}}{\text{Total area of peaks at 20.9°, 25.0°, and 26.3° of the reference sample}} \times 100$$

The porous structure and specific surface area based on the Brunauer-Emmett-Teller (BET) equation were determined by N_2 physisorption measurement in a relative pressure (p/p_0) range of 0.005–0.995 at 77 K using an automated apparatus (BELSORP-mini II, MicrotracBEL). Before physisorption measurements, each sample was heat-treated at 673 K for 1 h below 10 Pa using BELPREP VACII (MicrotracMRB). The BET equation was employed for the estimation of specific surface area (S_{BET}) in the appropriate p/p_0 range of adsorption branch where the C value in this equation becomes positive. The total pore volume (V_{total}) was evaluated from each adsorption branch at $p/p_0 = 0.95$.

The size and morphology of the particles were observed by field emission scanning electron microscope (FE-SEM; S-4800, Hitachi High-Tech, accelerating voltage 5.0 kV). The nature of the Ga and Si atoms was elucidated by solid-state ^{71}Ga magic angle spinning nuclear magnetic resonance spectroscopy (^{71}Ga MAS NMR) and ^{29}Si MAS NMR spectroscopy with/without the cross polarization (CP) technique using an NMR spectrometer (JNM-ECZL600G, JEOL, ^{71}Ga 183 MHz, ^{29}Si 119 MHz, MAS frequency 15 kHz, ZrO_2 rotor

size 3.2 mm). The data were managed using the JEOL Delta version 5.3.3 software for phase correction and OriginPro 2022b version 9.9.5.167 software for deconvolution with Voigt functions.

5. Temperature-programmed desorption measurement

The acidic nature of [Ga]-CHA samples was examined by temperature-programmed desorption (TPD) measurement. Prior to the measurement, the ion-exchange treatment was conducted for [Ga]-CHA to introduce NH_4^+ cations onto ion-exchange sites. Thus, 400 mg of [Ga]-CHA was dispersed in 100 mL of an aqueous NH_4NO_3 solution (2 M). The suspension was ultrasonicated for 1 min to disperse the zeolite particles well and magnetically stirred at 353 K for 3 h, followed by centrifugation and drying at 333 K overnight. This procedure was repeated twice.

The thus-prepared samples were subjected to the TPD measurement using an automated instrument (BELCAT II, MicrotracMRB, equipped with a quadrupole mass spectrometer (Q-MS; MicrotracMRB, BELMASS) and thermal conductivity detector (TCD)). Each sample (*ca.* 50 mg) charged in the apparatus was initially pretreated in an Ar flow (50 mL min^{-1}) at 373 K for 1 h. Note that although typical NH_3-TPD measurement involves the step of NH_3 adsorption in pretreatment procedure,[S7–S9] the current did not require such step because NH_4^+ species were already present on ion-exchange sites of each sample, which is the same situation for H^+-type zeolites after their exposure to NH_3. Afterwards, the temperature increased from 373 K to 1273 K at a ramp rate of 10 K min^{-1} under an Ar flow (30 mL min^{-1}). The acquired profiles were managed using the MicrotracBEL ChemMaster version 1.6.2 software for baseline correction and OriginPro 2022b version 9.9.5.167 software for deconvolution with Voigt functions.

6. Ion-exchange of Co^{2+} over [Ga]-CHA zeolites

To prevent the effects of a class of counter cations, each [Ga]-CHA zeolite sample was subjected to ion-exchange treatment prior to the Co^{2+} exchange experiment. Thus, 100 mg of [Ga]-CHA zeolite was dispersed in 30 mL of an aqueous NH_4NO_3 solution (2 M). The suspension was ultrasonicated for 1 min to achieve a better dispersion of the zeolite particles and stirred at 353 K for 3 h. After separation and washing with distilled water by centrifugation, the resulting sample was treated in the same manner once more. After the procedure, the sample was dried at 333 K overnight to yield [Ga]-CHA zeolite sample containing NH_4^+ as counter cation.

The exchange of Co^{2+} over **CHA**-type zeolites was conducted in the same manner as the procedure reported previously.[S5] 10 mg of the thus-prepared [Ga]-CHA zeolite sample containing NH_4^+ was dispersed in 10 mL of an aqueous $Co(NO_3)_2•6H_2O$ solution (50 mM). After ultrasonication to improve the dispersion of [Ga]-CHA zeolite particles, the suspension was stirred in an oil bath at 353 K for 3 h. After separation and washing with distilled water by centrifugation, the resulting sample was treated in the same manner once more. The resulting powder was dried at 333 K overnight. The 50 mg of the thus-prepared sample containing Co^{2+} was dissolved completely in an aqueous mixture of HNO_3 (0.5 M, 4 mL) and HF (47–49 wt%, 3 mL) at room temperature and diluted with distilled water in a 50 mL volumetric flask. The solution was further diluted 10 times with distilled water and analyzed by ICP-OES.

The Co-exchanged samples were also analyzed by diffuse-reflectance ultraviolet-visible spectroscopy (DR-UV-vis; H-3900, Hitachi) and Co *K*-edge X-ray absorption spectroscopy (XAS). For DR-UV-vis spectroscopy, $BaSO_4$ was used as a background. XAS was operated at the SPring-8 BL14B2 beamline

(Proposal No. 2023B1740; ring energy 8.0 GeV, ring current 100 mA, equipped with a Si(111) double-crystal monochromator). Authentic samples (Co powder, $Co(OH)_2$, CoO, and Co_3O_4) and Co-exchanged samples were analyzed with the transmission mode, where the I_0 and I_1 ion chambers were filled with 100 vol% N_2 and 20 vol% Ar/N_2, respectively. Each authentic (or Co-exchanged) sample was mixed and ground well in a mortar with boron nitride, and the mixture was pelletized prior to the XAS measurement. The acquired spectra were analyzed using REX2000 software version 2.6.0 (Rigaku). The Co *K*-edge extended X-ray absorption fine structure (EXAFS) oscillations were extracted from the raw XAS data in the k range of 3–12. The empirical phase shift and amplitude function for the Co–O shell were calculated with the FEFF8.2 program.

[Discussion about the effect of duration of hydrothermal treatment]

The hydrothermal treatment for the thus-prepared Ga-rich silica-gallia was conducted with the different duration to synthesize [Ga]-CHA samples; in this investigation, the aging time of t_2 was kept constant at 9 h (*i.e.*, the series of [Ga]-CHA-9 specimens were synthesized; see Experimental and Fig. S1). The XRD patterns for the samples synthesized with the duration of hydrothermal treatment of 5 h or longer were consistent with that of chabazite (Fig. S3A), indicating the successful construction of **CHA**-type frameworks from the Ga-rich silica-gallia without formation of other type of frameworks or gallium oxides. The progress of crystallization monitored by XRD was drawn as the relative crystallinity curve, as shown in Fig. S3B. The crystallization did not occur within the hydrothermal treatment time of 4 h or shorter while proceeded rapidly between 4–5 h. The relative crystallinity reached maxima at the hydrothermal duration of 72 h. The solid yield and Si/Ga molar ratio of prepared samples increased along with the progress of crystallization upon the increased duration of hydrothermal treatment and reached 70% and 6.0, respectively. These data indicated that a large portion of Si- and Ga-containing species was initially dissolved in the basic solution composed of TMAdaOH and NaOH and precipitated as **CHA**-type zeolites once enough amount of nuclei was accumulated in the synthesis gel. This behavior was also suggested by the SEM images (Fig. S4), where small nuclei attached on huge stone-like particles were found at short duration of hydrothermal treatment (namely at 3 h) and crystalline particles appeared at the hydrothermal duration of 5 h or longer. Also, the gap between the actual Si/Ga ratio of 6.0 and the ratio of original synthesis gel (*i.e.*, 10; see Experimental) indicated that Si species still remained dissolved in the solution. Another important observation was the sample color after the calcination at 873 K for 12 h. The color of [Ga]-CHA-t_2 samples prepared at the hydrothermal duration of 3–6 h was grey or black, while that synthesized at the duration of 24 h or longer was white. This change in the sample color indicated that the construction of **CHA**-type framework during the hydrothermal treatment for 6 h or shorter was not enough, and TMAdaOH molecules used as an organic SDA could not undergo the combustion to be evacuated from the precipitate and instead were carbonized during the calcination treatment. We should note that the hydrothermal treatment for the mixture of TEOS and $Ga(NO_3)_3$ under the same conditions failed to yield **CHA**-type framework, demonstrating that the use of the Ga-rich silica-gallia is the key to the construction of **CHA**-type framework.

These samples were further analyzed by solid-state NMR spectroscopy to elucidate the nature of Si and Ga species. The ^{71}Ga MAS NMR spectra (Fig. S5A) indicated that only tetrahedral Ga species were present in all the samples regardless of the hydrothermal duration due to the presence of signal at 168 ppm and the absence of signal at *ca.* 0 ppm, the latter of which is assignable to octahedral Ga species in the zeolite pores (*i.e.*, extra-framework Ga species).[S10,S11] Given that the dominant Ga species involved in the Ga-rich silica-gallia was octahedra, the coordination geometry of Ga species was altered to be tetrahedra at the initial stage of hydrothermal process. The growing intensity and sharpness of the peak at 168 ppm upon the hydrothermal duration can be rationalized by the improvement of crystallinity of **CHA**-type framework, which possesses single crystallographically distinct T-sites and thus provides the NMR signal at the same position in stark contrast to amorphous materials that provide peaks at different positions. Due to the same reason, the signals observed in the ^{29}Si MAS NMR spectra became more prominent at the longer hydrothermal duration (Fig. S5B). In these spectra, three signals appeared at –111, –103, and –95 ppm, which were attributable to Q^4(0Ga), Q^4(1Ga), and Q^4(2Ga) species, respectively.[S12] Meanwhile, no obvious peak was observed in the ^{29}Si CP/MAS

NMR spectra (Fig. S5C), and thus, defect sites were negligible in these materials. This fact allowed us to evaluate the proportion of Q^4(nGa) species in the synthesized material by deconvoluting their ^{29}Si MAS NMR spectra without consideration of overlap with defect-derived peaks. These data thus demonstrated the formation of paired Ga sites (*i.e.*, Q^4(2Ga) species) by the current synthetic approach. Based on this insight, the proportion of Q^4(nGa) species was evaluated for the four samples that exhibited the high relative crystallinity (*i.e.*, the samples synthesized with the hydrothermal duration of 24–168 h), The deconvoluted spectra and calculated proportion of Q^4(nGa) species are shown in Fig. S6 and Table S2, respectively. The difference in the proportion of Q^4(2Ga) species in the Ga-containing Q^4(nGa) (n = 1 or 2) species was in a narrow range (18–21%) regardless of the hydrothermal treatment time. This trend pointed out that the duration of hydrothermal treatment did not affect the formation of Q^4(2Ga) species in the **CHA**-type framework in the current synthetic technique. In this study, 72 h was determined as the optimum hydrothermal duration because of the high relative crystallinity and solid yield.

[Discussion about the acidic nature of [Ga]-CHA-t_2 samples]

The acidic nature of [Ga]-CHA-t_2 samples was examined by TPD measurement. As seen in the TPD profiles depicted in Fig. S11, two desorption peaks were observed at 743 K and 1003 K. The former peak was attributable to the NH_3 species desorbed from Brønsted-acid sites. The latter was originated from NH_3 species captured by Lewis-acid sites that were generated via the degalliation in the TPD measurements, because extraframework Ga species on silicate surfaces were previously reported to generate strong Lewis-acid sites.[S13] For all the [Ga]-CHA-t_2 samples, the total amount of acid sites as well as desorption temperature were similar to each other regardless of the difference in the proportion of Q^4(2Ga) species (= paired Ga sites) (Table S3). The total amount of acid sites was close to half of the Ga content in [Ga]-CHA-t_2; perhaps, the narrow pores of **CHA**-type zeolites could hamper the mass transfer during the ion-exchange treatment.

The quantity of strong Lewis-acid sites was apt to be higher in the cases of [Ga]-CHA-t_2 samples with the higher Q^4(2Ga) proportion. This trend indicated the lower thermal stability of paired Ga sites compared to isolated Ga species. Such lower stability of paired Ga sites will be the drawback for the catalytic use of [Ga]-CHA-t_2 samples as they are, yet the construction of paired Ga sites and subsequent degalliation shown here may be a useful approach to generating zeolite catalysts enriched with strong Lewis-acid sites.

Table S1. Reported intentional formation of paired heteroatom (M) sites in zeolite frameworks.[a]

Sample name in each report	Framework type	M	Strategy for the formation of paired heteroatom sites	Source(s)		SDA(s)	Si/M ratio	Max. prop. of $Q^4(2M)$[b] /%	2 × M'^{2+}/M ratio[c]	Ref.
				Si	Heteroatom (Al or Ga)					
ZSM-5	**MFI**	Al	Optimized combination of Si and Al sources	TEOS	$AlCl_3$	TPA^+	28	–	0.33 (Co^{2+})	S14
ZSM-5 (from mixture series **C**)	**MFI**	Al	Optimized combination of Si and Al sources	TEOS	$AlCl_3$	TPA^+	25	33	0.70 (Co^{2+})	S15
SSZ-13(15, 1.00)	**CHA**	Al	Electrostatic interaction given by large and small SDAs	Colloidal silica	$Al(OH)_3$	$TMAda^+$ + Na^+	14.8	–	0.08 (Co^{2+})	S16
None	**CHA**	Al	Electrostatic interaction given by large and small SDAs	Colloidal silica	$Al(OiPr)_3$	$TMAda^+$ + Na^+	15.0	–	0.44 (Co^{2+})	S17, S18
CHA-F-1.0	**CHA**	Al	Transcription of paired species from zeolite	**FAU**-type zeolite (Si/Al = 2.8) + fumed silica	**FAU**-type zeolite (Si/Al = 2.8)	$TMAda^+$ + Na^+	13.5	30	–	S19
CHA-FAU-TEA	**CHA**	Al	Transcription of paired species from zeolite	**FAU**-type zeolite (Si/Al = 2.4) + fumed silica	**FAU**-type zeolite (Si/Al = 2.4)	$TMAda^+$ + Na^+	6.3	18	–	S20
CHA-9	**CHA**	Al	Transcription of paired species from amorphous precursor	Al-rich amorphous silica-alumina (Si/Al = 2.5) + silica gel	Al-rich amorphous silica-alumina (Si/Al = 2.5)	$TMAda^+$ + Na^+	5.7	23	0.60 (Sr^{2+})	S4
MFI-9	**MFI**	Al	Transcription of paired species from amorphous precursor	Al-rich amorphous silica-alumina (Si/Al = 2.5) + silica gel	Al-rich amorphous silica-alumina (Si/Al = 2.5)	TPA^+ + Na^+	11	–	0.36 (Co^{2+})	S5
[Ga]-CHA-9	**CHA**	Ga	Transcription of paired species from amorphous precursor	Ga-rich amorphous silica-gallia (Si/Ga = 1.9) + silica gel	Ga-rich amorphous silica-gallia (Si/Ga = 1.9)	$TMAda^+$ + Na^+	5.7	19	0.60 (Co^{2+})	This work

[a]Abbreviations: SDA = structure-directing agent; TEOS = tetraethyl orthosilicate; O*i*Pr = isopropoxide; TPA^+ = tetrapropylammonium cation; $TMAda^+$ = *N*,*N*,*N*-trimethyl-1-adamantylammonium cation.

[b]Maximum proportion of $Q^4(2M)$ in the total M-containing $Q^4(nM)$ (n = 1 and 2; M = isomorphously substituting heteroatom), estimated by ^{29}Si MAS NMR spectroscopy: from the areas of each $Q^4(2M)$ peak in ^{29}Si MAS NMR spectra, *i.e.*, (Proportion of M-containing $Q^4(nM)$) = (Peak area for $Q^4(nM)$) / ((Peak area for $Q^4(1M)$) + (Peak area for $Q^4(2M)$)).

[c]Determined via ion-exchange using divalent cation M'^{2+} shown in the parentheses (*i.e.*, either Co^{2+} or Sr^{2+}). Both the second nearest neighboring pair (Al–O–Si–O–Al sequence, consistent with $Q^4(2M)$) and third nearest neighboring pair (Al–O–Si–O–Si–O–Al sequence) are counted by this method.

Table S2. Effect of hydrothermal duration on properties of [Ga]-CHA-9.[a]

Hydrothermal duration /h	Solid yield[b] /%	Si/Ga ratio[c]	Proportion of Q^4(nGa)[d] /%			Proportion of Ga-containing Q^4(nGa)[e] /%	
			Q^4(0Ga)	Q^4(1Ga)	Q^4(2Ga)	Q^4(1Ga)	Q^4(2Ga)
24	66	5.4	52 ± 1	38 ± 1	10 ± 0	79 ± 1	21 ± 0
72	69	5.7	59 ± 1	33 ± 1	7.9 ± 0.2	81 ± 2	19 ± 1
120	73	6.1	55 ± 1	37 ± 1	8.4 ± 0.2	81 ± 2	19 ± 1
168	73	6.1	59 ± 1	34 ± 1	7.4 ± 0.2	82 ± 2	18 ± 1

[a]Synthesis conditions: aging, room temperature, t_1 = 37 h, t_2 = 9 h; hydrothermal treatment, 443 K, 24–168 h, 40 rpm; Si/Ga/NaOH/TMAdaOH/H_2O = 1/0.10/0.44/0.20/30.

[b]Calculated by dividing the mass of each calcined [Ga]-CHA-t_2 sample by the total mass of the dried starting reagents (*i.e.*, silica-gallia, SiO_2, and seed crystal).

[c]Determined via ICP-OES.

[d]Estimated from the areas of each Q^4(nGa) peak in the ^{29}Si MAS NMR spectra (Figs. S5B and S6): (Proportion of Q^4(nGa (n = 0–2)) = (Peak area for Q^4(nGa))/((Peak area for Q^4(0Ga)) + (Peak area for Q^4(1Ga)) + (Peak area for Q^4(2Ga))).

[e]Estimated from the areas of each Q^4(nGa) peak in the ^{29}Si MAS NMR spectra (Figs. S5B and S6): (Proportion of Ga-containing Q^4(nGa (n = 1 or 2)) = (Peak area for Q^4(nGa))/((Peak area for Q^4(1Ga)) + (Peak area for Q^4(2Ga))).

Table S3. Acidic nature of [Ga]-CHA-t_2 samples.

Sample[a]	Si/Ga ratio[b]	Proportion of Q^4(nGa)[c] /%			Proportion of Ga-containing Q^4(nGa)[d] /%		Desorbed NH_3[e] /mmol g^{-1}		
		Q^4(0Ga)	Q^4(1Ga)	Q^4(2Ga)	Q^4(1Ga)	Q^4(2Ga)	743 K	1003 K	Total
[Ga]-CHA-0	5.5	64 ± 2	32 ± 1	3.7 ± 0.1	90 ± 3	10 ± 0	1.00	0.17	1.17
[Ga]-CHA-3	5.5	58 ± 1	36 ± 1	5.5 ± 0.2	87 ± 2	13 ± 0	0.96	0.17	1.13
[Ga]-CHA-6	5.5	62 ± 1	32 ± 1	6.2 ± 0.2	84 ± 2	16 ± 1	1.05	0.30	1.35
[Ga]-CHA-9	5.7	59 ± 1	33 ± 1	7.9 ± 0.2	81 ± 2	19 ± 1	0.82	0.39	1.21
[Ga]-CHA-12	5.5	58 ± 1	36 ± 1	6.7 ± 0.2	84 ± 2	16 ± 0	1.00	0.25	1.25
[Ga]-CHA-24	5.5	57 ± 1	37 ± 1	6.1 ± 0.2	86 ± 2	14 ± 0	0.92	0.29	1.21

[a]Synthesis conditions: aging, room temperature, t_1 = 24–48 h, t_2 = 0–24 h (t_1 + t_2 = 48 h); hydrothermal treatment, 443 K, 72 h, 40 rpm; Si/Ga/NaOH/TMAdaOH/H_2O = 1/0.10/0.44/0.20/30.

[b]Determined via ICP-OES.

[c]Estimated from the areas of each Q^4(nGa) peak in the ^{29}Si MAS NMR spectra (Figs. S9B and S10): (Proportion of Q^4(nGa (n = 0–2)) = (Peak area for Q^4(nGa))/((Peak area for Q^4(0Ga)) + (Peak area for Q^4(1Ga)) + (Peak area for Q^4(2Ga))).

[d]Estimated from the areas of each Q^4(nGa) peak in the ^{29}Si MAS NMR spectra (Figs. S9B and S10): (Proportion of Ga-containing Q^4(nGa (n = 1 or 2)) = (Peak area for Q^4(nGa))/((Peak area for Q^4(1Ga)) + (Peak area for Q^4(2Ga))).

[e]Eludicated from TPD profiles (Fig. S11). The displayed temperature value indicates the temperature which gave the maximum height of each peak.

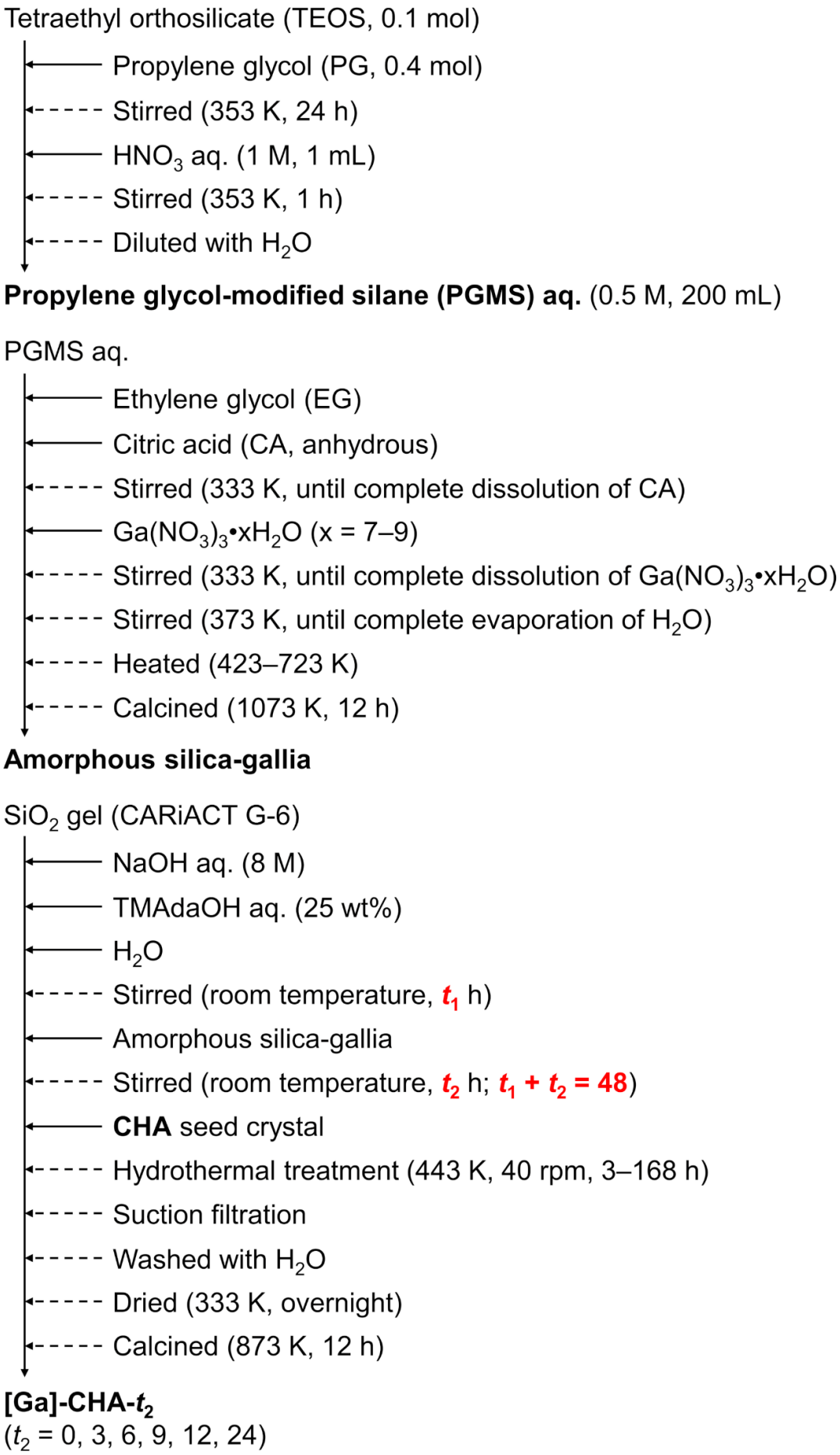

Fig. S1. Procedure of transcription-induced method for synthesizing [Ga]-CHA-t_2 samples.

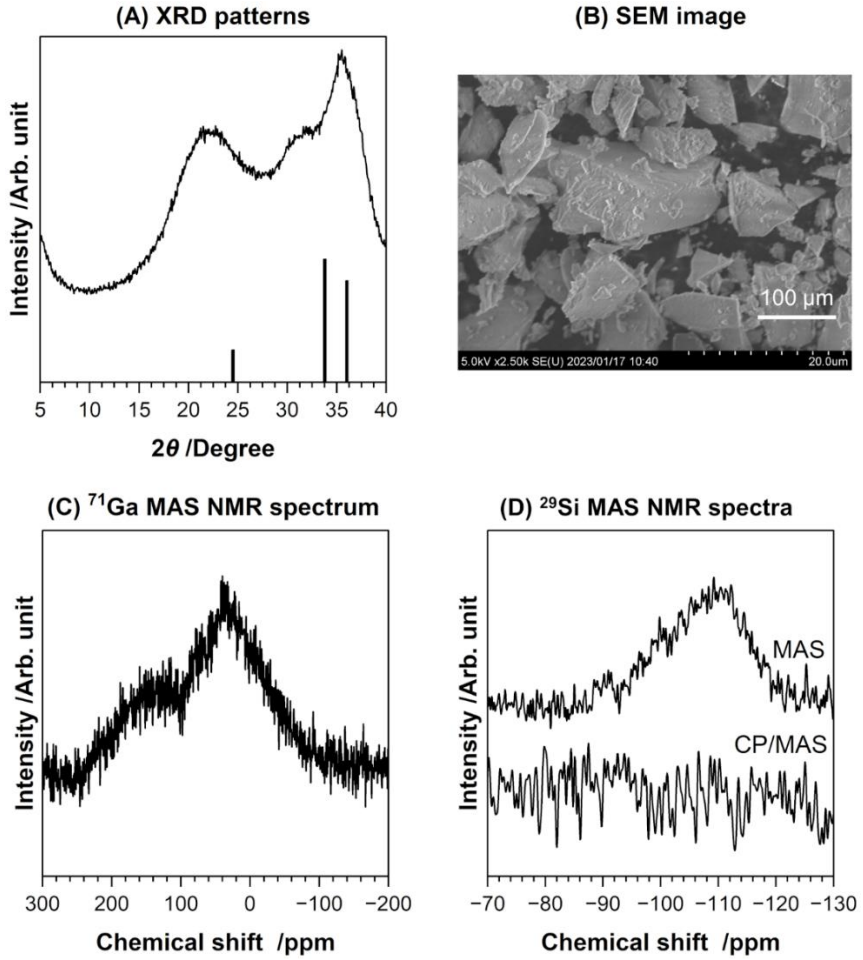

Fig. S2. Characterization data of Ga-rich amorphous silica-gallia prepared via the Pechini method: (A) XRD pattern, (B) SEM image; (C) ^{71}Ga MAS NMR spectrum; and (D) ^{29}Si MAS NMR and ^{29}Si CP/MAS NMR spectra. Reference for XRD: α-Ga_2O_3 (ICSD card #27431), β-Ga_2O_3 (PDF card #04-013-1344).

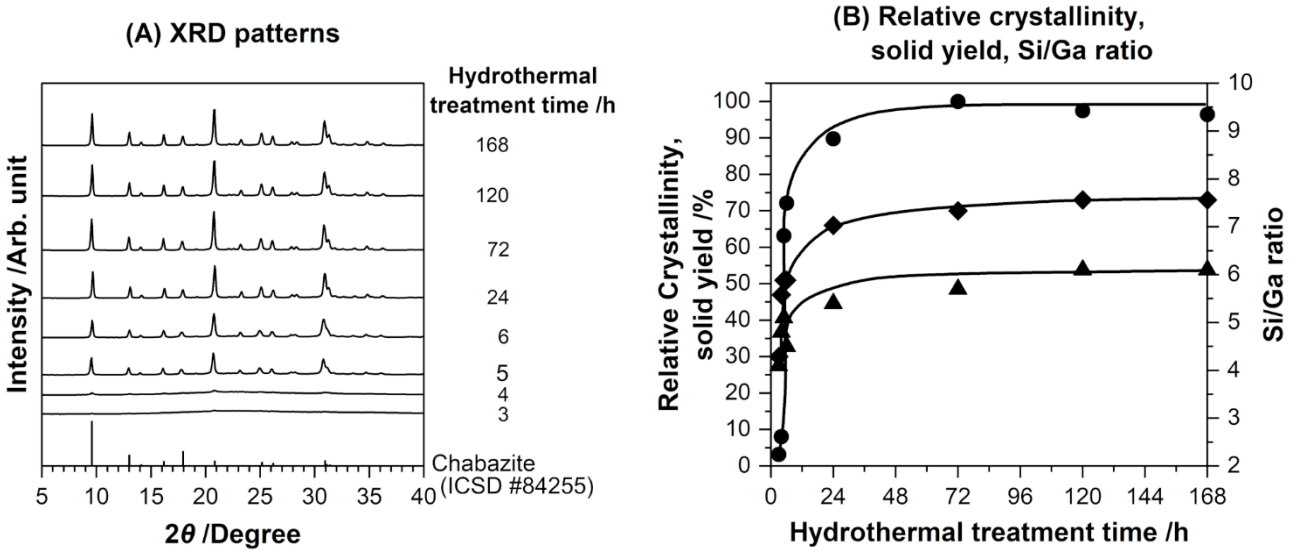

Fig. S3. (A) XRD patterns of [Ga]-CHA-9 synthesized at different hydrothermal duration (3–168 h). Reference: chabazite (**CHA**-type zeolite, ICSD card #84255). (B) Relative crystallinity curve (circles) of [Ga]-CHA-9 with solid yield (diamonds) and Si/Ga ratio (triangles)**.**

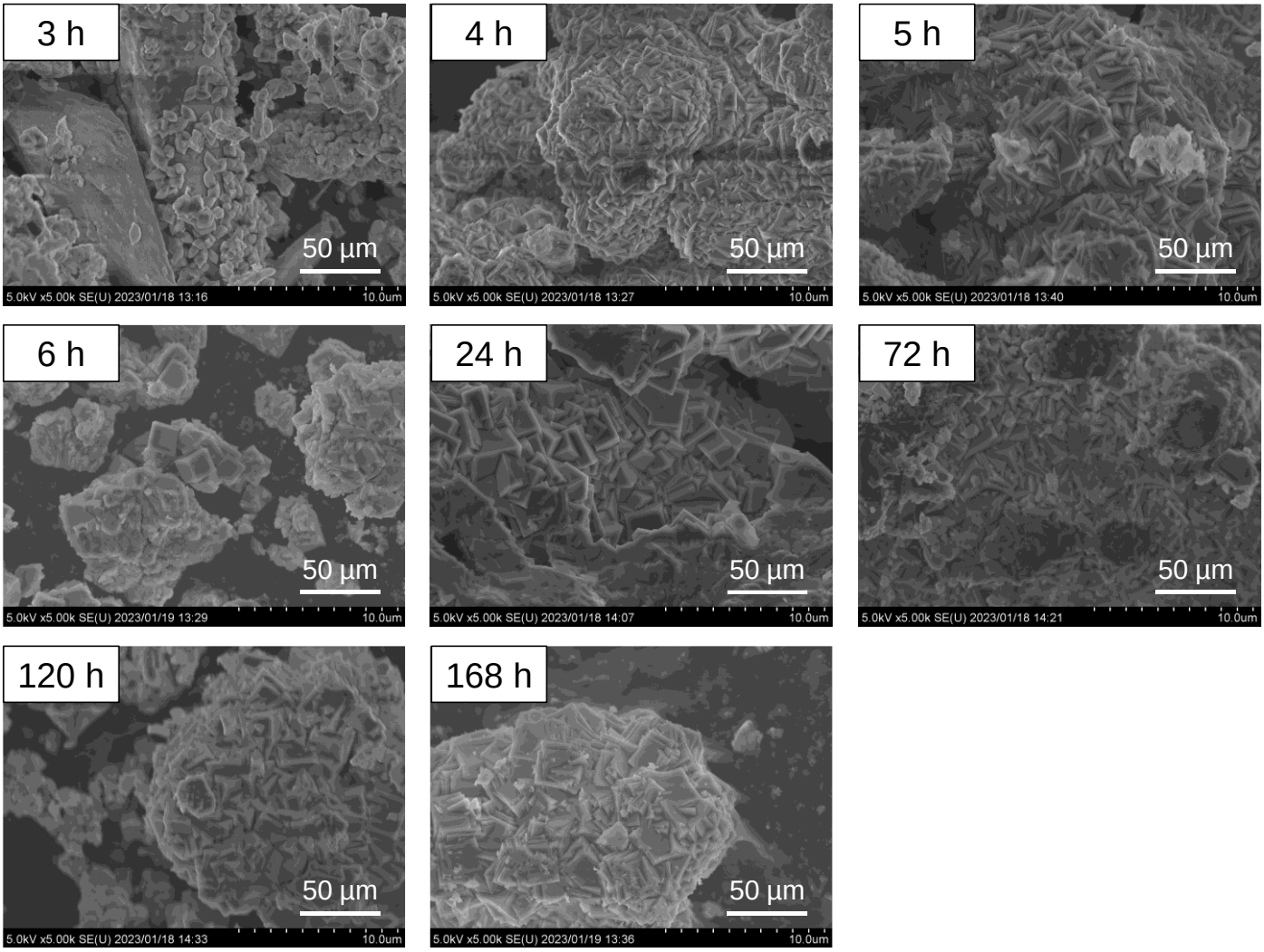

Fig. S4. Morphology of the particles of [Ga]-CHA-9 synthesized at different hydrothermal duration (3–168 h), measured by SEM.

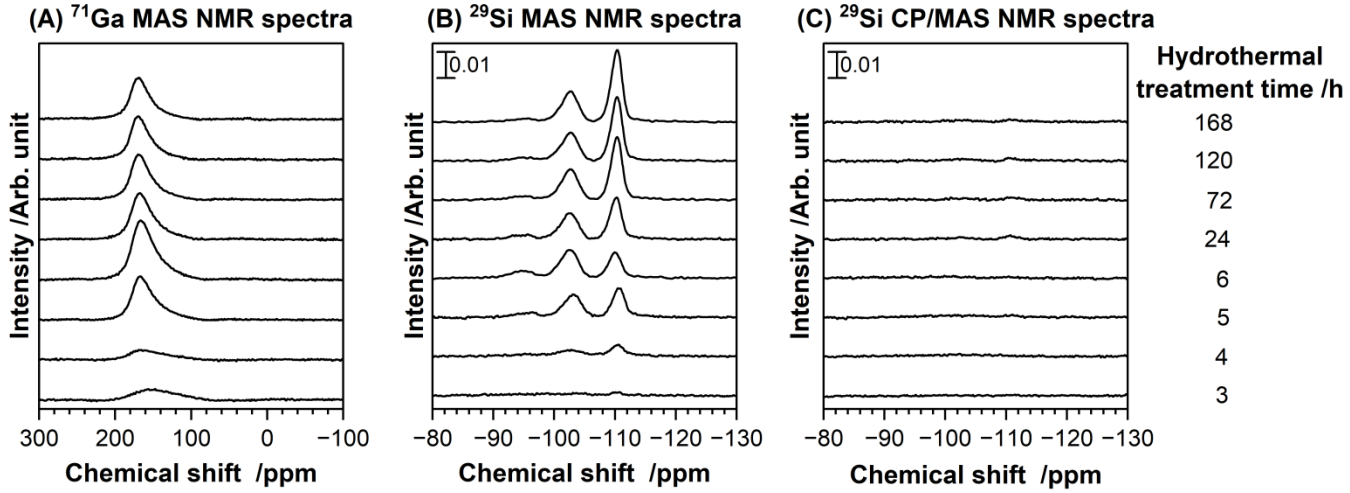

Fig. S5. Coordination structure of Ga and Si species involved in [Ga]-CHA-9 synthesized at different hydrothermal duration (3–168 h), examined by solid-state NMR spectroscopy: (A) ^{71}Ga MAS NMR; (B) ^{29}Si MAS NMR; and (C) ^{29}Si CP/MAS NMR. The deconvoluted results for the figure B are depicted in Fig. S6.

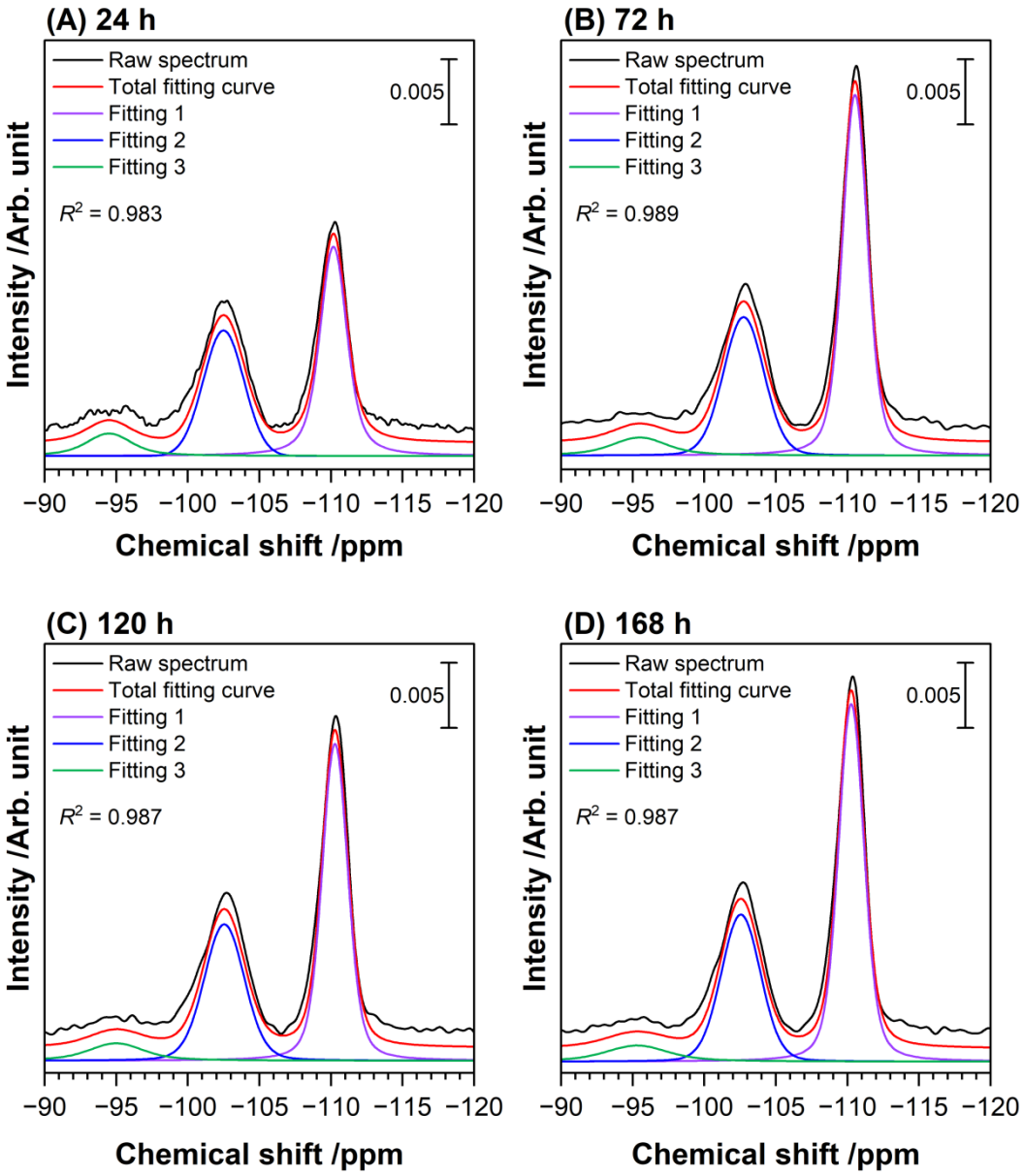

Fig. S6. Deconvolution curves for the ^{29}Si MAS NMR spectra of [Ga]-CHA-9 synthesized at different hydrothermal duration: (A) 24 h; (B) 72 h; (C) 120 h; (D) 168 h. For the ease of viewing, the baselines for raw spectrum (black line) and total fitting curve (red line) were shifted vertically.

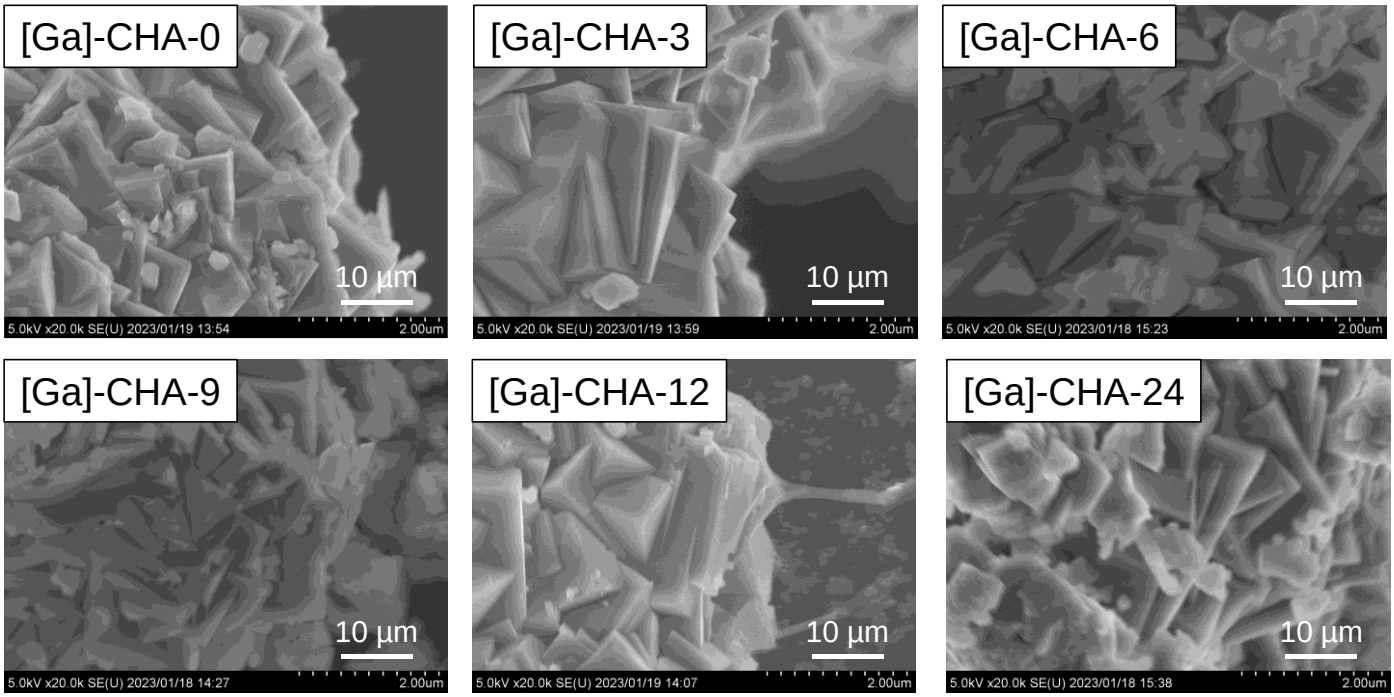

Fig. S7. Morphology of the particles of [Ga]-CHA-t_2 samples (t_2 = 0–24 h), measured by SEM.

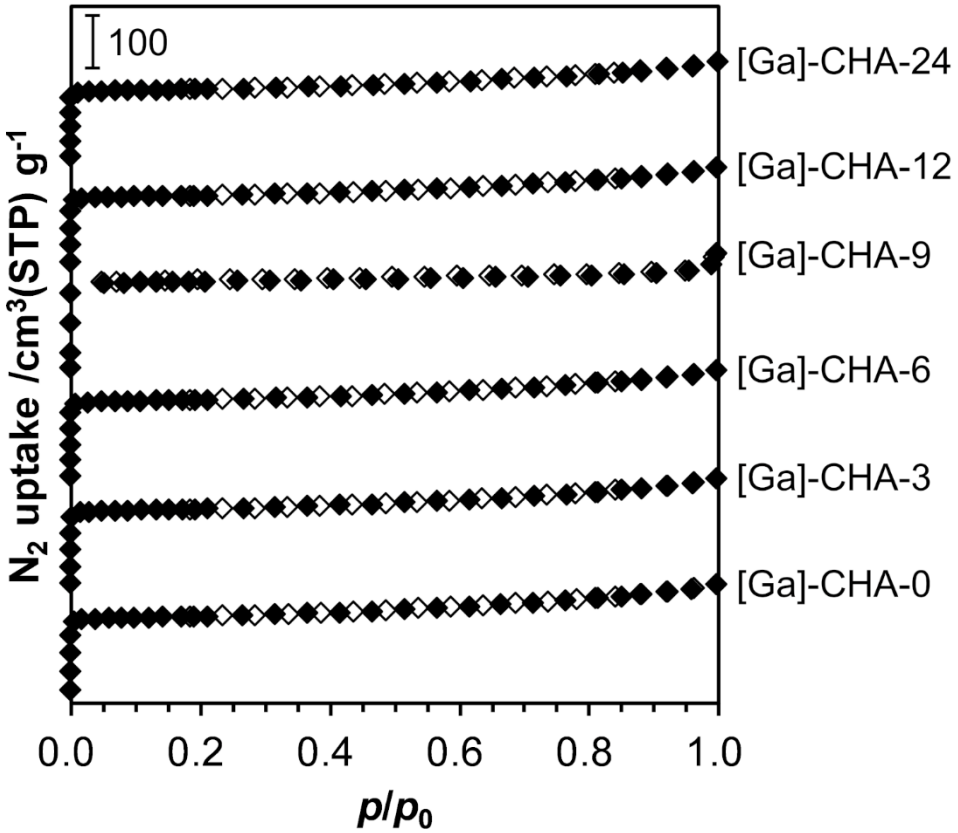

Fig. S8. N_2 physisorption isotherms for [Ga]-CHA-t_2 synthesized at different aging time (t_2 = 0–24 h). Legends: filled dots = adsorption branch; open dots = desorption branch. The BET specific surface area and total pore volume estimated from each isotherm are summarized in Table 1.

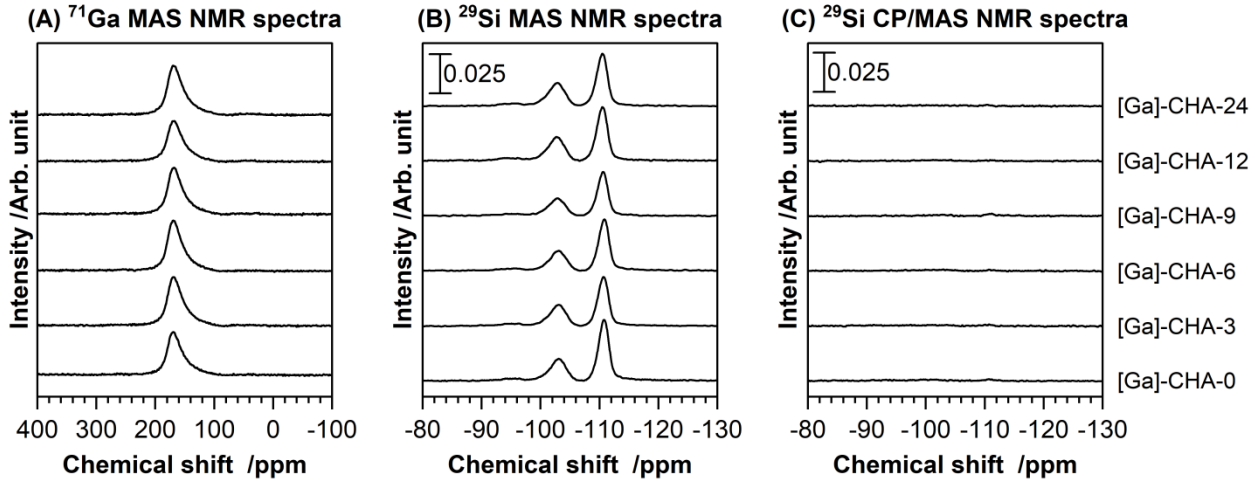

Fig. S9. Coordination structure of Ga and Si species involved in [Ga]-CHA-t_2 (t_2 = 0–24 h), examined by solid-state NMR spectroscopy: (A) ^{71}Ga MAS NMR; (B) ^{29}Si MAS NMR; and (C) ^{29}Si CP/MAS NMR. The deconvoluted results for the figure B are depicted in Fig. S10.

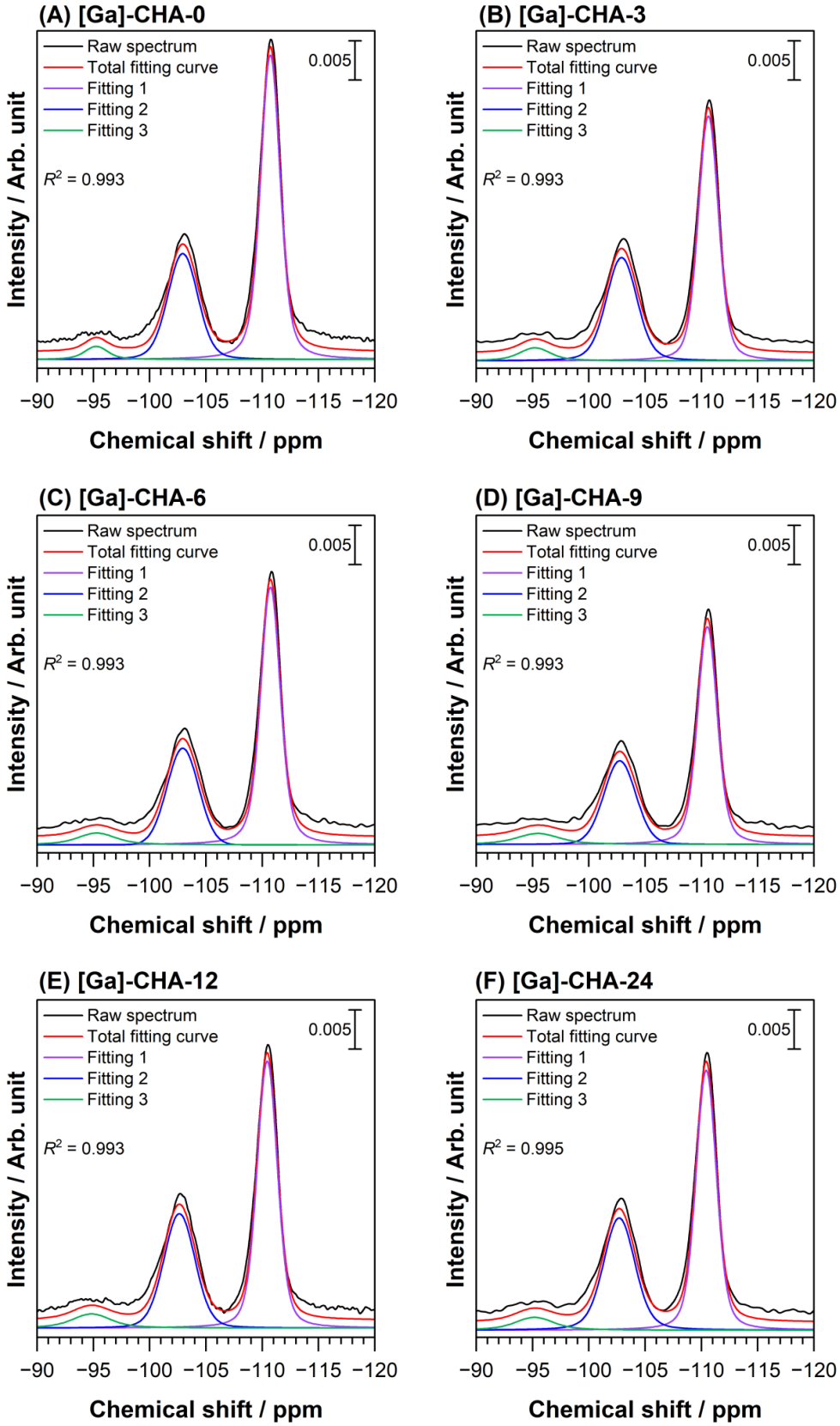

Fig. S10. Deconvolution curves for ^{29}Si MAS NMR spectra of [Ga]-CHA-t_2 synthesized at different aging time (t_2 = 0–24 h): (A) [Ga]-CHA-0; (B) [Ga]-CHA-3; (C) [Ga]-CHA-6; (D) [Ga]-CHA-9; (E) [Ga]-CHA-12; (F) [Ga]-CHA-24. For the ease of viewing, the baselines for raw spectrum (black line) and total fitting curve (red line) were shifted vertically.

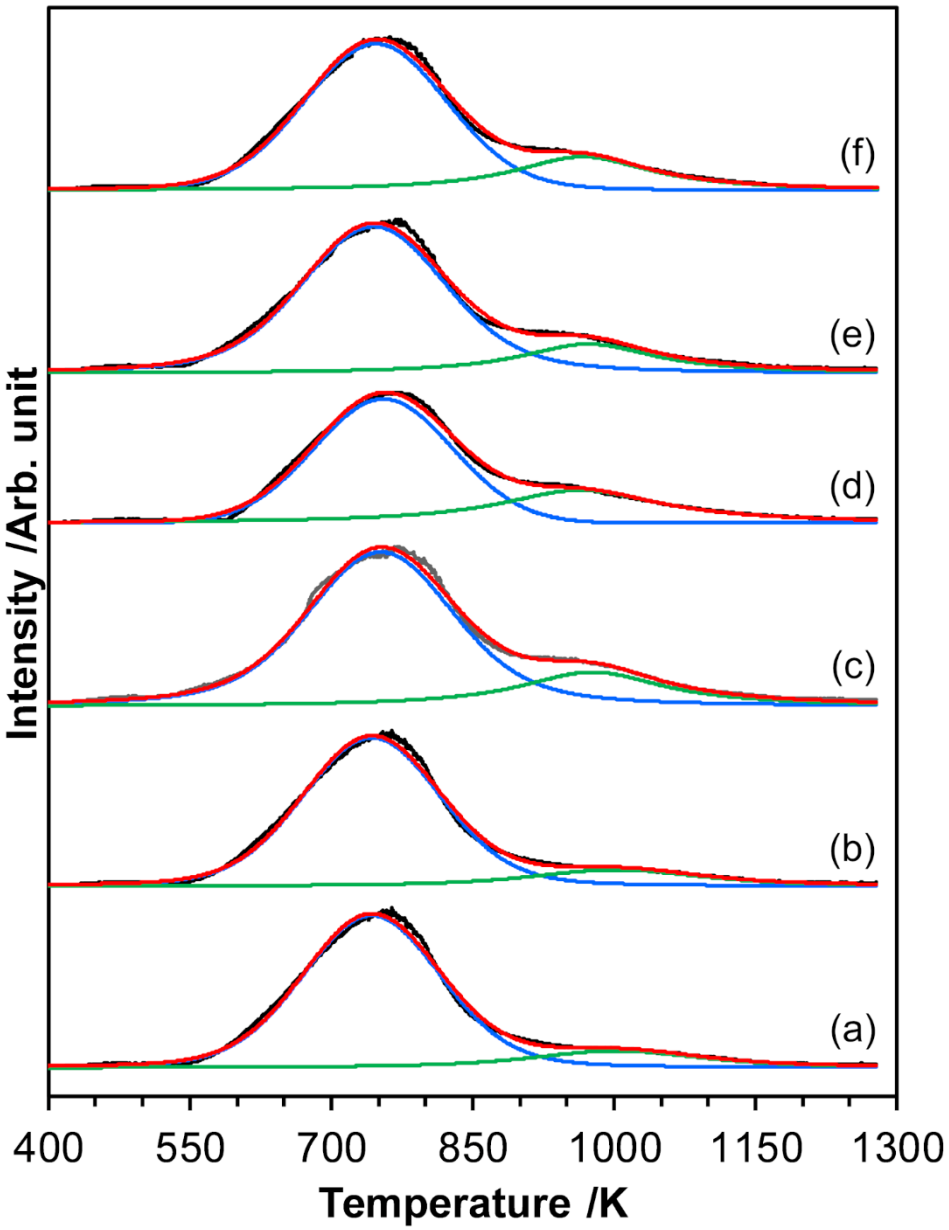

Fig. S11. TPD profiles for [Ga]-CHA-t_2 samples, recorded with Q-MS at m/z = 16. Analysis conditions: NH_4^+-type [Ga]-CHA-t_2 *ca.* 50 mg; Ar flow 30 mL min^{-1}; 10 K min^{-1}; 373–1273 K. The quantification data are summarized in Table S3. For each profile, the raw profile (black line) and fitting curves (fitting curve 1 (blue), fitting curve 2 (green), and total fitting curve (red)) are shown together.

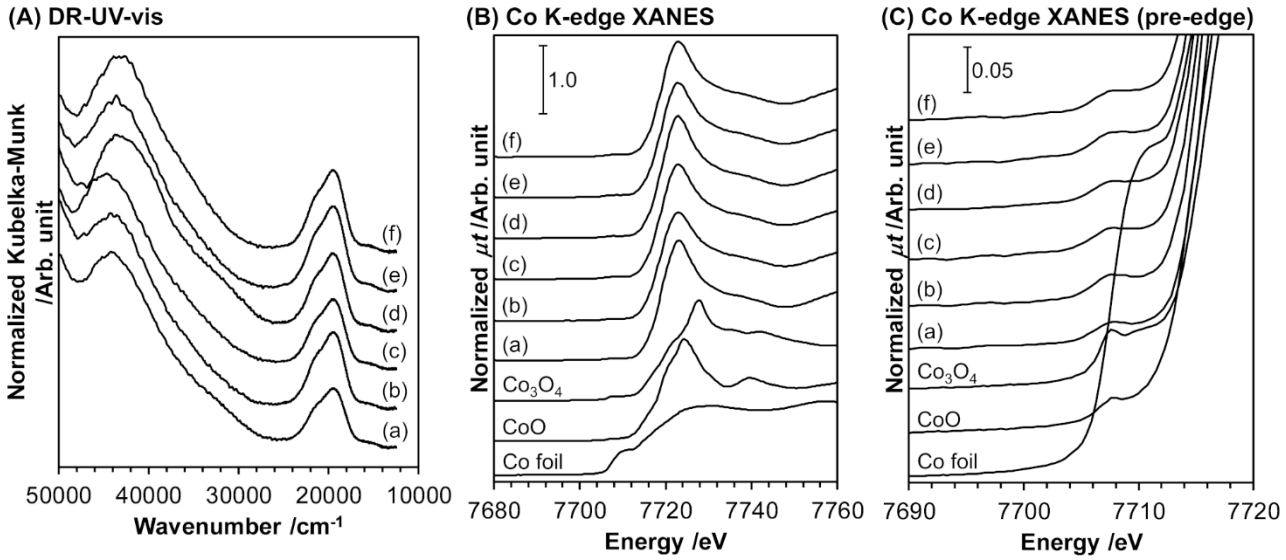

Fig. S12. Spectroscopic data for Co^{2+}-exchanged [Ga]-CHA-t_2 samples: (A) DR-UV-vis spectra; (B) Co *K*-edge XANES spectra; (C) enlarged view of figure B. Legends: (a) Co^{2+}/[Ga]-CHA-0; (b) Co^{2+}/[Ga]-CHA-3; (c) Co^{2+}/[Ga]-CHA-6; (d) Co^{2+}/[Ga]-CHA-9; (e) Co^{2+}/[Ga]-CHA-12; (f) Co^{2+}/[Ga]-CHA-24.

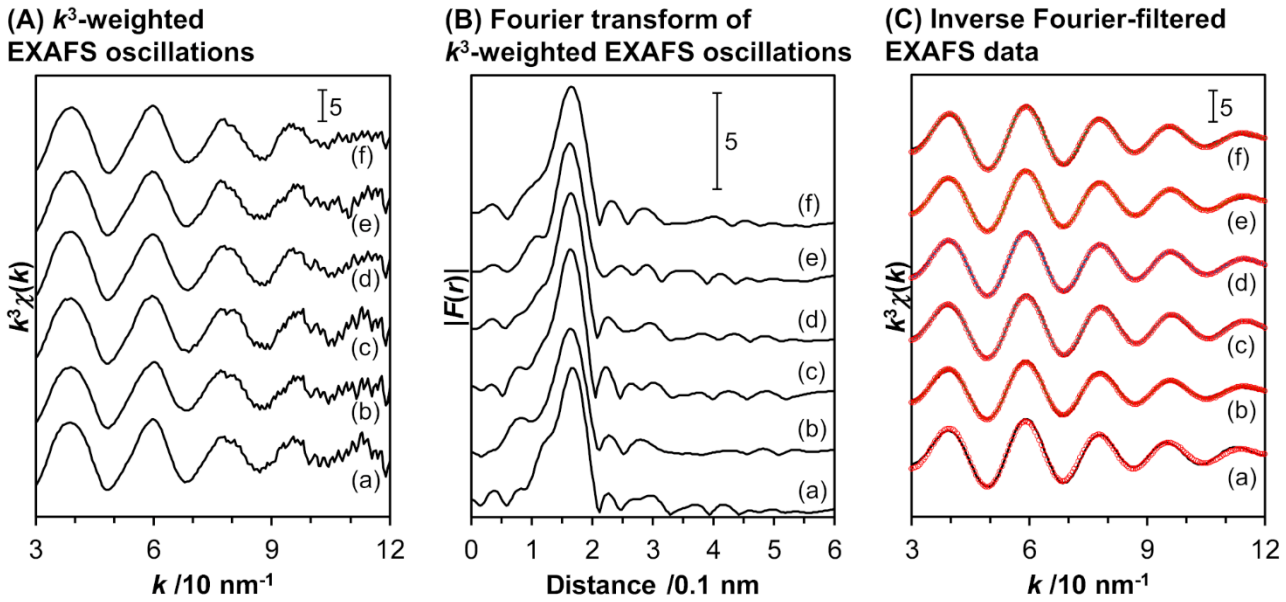

Fig. S13. Co *K*-edge EXAFS data for Co^{2+}-exchanged [Ga]-CHA-t_2 samples: (A) k^3-weighted EXAFS oscillations; (B) Fourier transform of k^3-weighted EXAFS oscillations; (C) inverse Fourier-filtered EXAFS data (black solid lines) with fitted data (red open circles). Legends: (a) Co^{2+}/[Ga]-CHA-0; (b) Co^{2+}/[Ga]-CHA-3; (c) Co^{2+}/[Ga]-CHA-6; (d) Co^{2+}/[Ga]-CHA-9; (e) Co^{2+}/[Ga]-CHA-12; (f) Co^{2+}/[Ga]-CHA-24. The curve fitting results are summarized in Table 2.

Supplementary references

S1 M. P. Pechini, US Patent 3330697A, 1967.

S2 M. Kakihana and M. Yoshimura, *Bull. Chem. Soc. Jpn.*, 1999, **72**, 1427–1443.

S3 K. Yoshizawa, H. Kato and M. Kakihana, *J. Mater. Chem.*, 2012, **22**, 17272–17277.

S4 M. Yabushita, Y. Imanishi, T. Xiao, R. Osuga, T. Nishitoba, S. Maki, K. Kanie, W. Cao, T. Yokoi and A. Muramatsu, *Chem. Commun.*, 2021, **57**, 13301–13304.

S5 Y. Imanishi, R. Osuga, A. Muramatsu and M. Yabushita, *J. Jpn. Petrol. Inst.*, 2023, **66**, 246–253.

S6 T. Umeda, H. Yamada, K. Ohara, K. Yoshida, Y. Sasaki, M. Takano, S. Inagaki, Y. Kubota, T. Takewaki, T. Okubo and T. Wakihara, *J. Phys. Chem. C*, 2017, **121**, 24324–24334.

S7 R. Fujii, M. Yabushita, D. Asada, M. Tamura, Y. Nakagawa, A. Takahashi, A. Nakayama and K. Tomishige, *ACS Catal.*, 2023, **13**, 1562–1573.

S8 K. Onodera, Y. Nakaji, M. Yabushita, Y. Nakagawa and K. Tomishige, *Appl. Catal. A: Gen.*, 2023, **663**, 119321.

S9 S. Mihara, M. Yabushita, Y. Nakagawa and K. Tomishige, *ChemSusChem*, 2024, **17**, e202301436.

S10 A. P. M. Kentgens, C. R. Bayense, J. H. C. van Hooff, J. W. de Haan and L. J. M. van de Ven, *Chem. Phys. Lett.*, 1991, **176**, 399–403.

S11 C. R. Bayense, A. P. M. Kentgens, J. W. De Haan, L. J. M. Van de Ven and J. H. C. Van Hooff, *J. Phys. Chem.*, 1992, **96**, 775–782.

S12 N. Janes and E. Oldfield, *J. Am. Chem. Soc.*, 1985, **107**, 6769–6775.

S13 T. Miyamoto, N. Katada, J.-H. Kim and M. Niwa, *J. Phys. Chem. B.*, 1998, **102**, 6738–6745.

S14 V. Gábová, J. Dědeček and J. Čejka, *Chem. Commun.*, 2003, 1196–1197.

S15 J. Dedecek, V. Balgová, V. Pashkova, P. Klein and B. Wichterlová, *Chem. Mater.*, 2012, **24**, 3231–3239.

S16 J. R. Di Iorio and R. Gounder, *Chem. Mater.*, 2016, **28**, 2236–2247.

S17 J. R. Di Iorio, S. Li, C. B. Jones, C. T. Nimlos, Y. Wang, E. Kunkes, V. Vattipalli, S. Prasad, A. Moini, W. F. Schneider and R. Gounder, *J. Am. Chem. Soc.*, 2020, **142**, 4807–4819.

S18 P. M. Kester, J. T. Crum, S. Li, W. F. Schneider and R. Gounder, *J. Catal.*, 2021, **395**, 210–226.

S19 T. Nishitoba, N. Yoshida, J. N. Kondo and T. Yokoi, *Ind. Eng. Chem. Res.*, 2018, **57**, 3914–3922.

S20 T. Nishitoba, T. Nozaki, S. Park, Y. Wang, J. N. Kondo, H. Gies and T. Yokoi, *Catalysts*, 2020, **10**, 1204.